PHYSICAL REVIEW D VOLUME 17, NUMBER 11 1 JUNE 1978

s-dependence of proton fragmentation by hadrons. II. Incident laboratory momenta 30–250 GeV/c

H. Weisberg
Accelerator Department, Brookhaven National Laboratory, Upton, New York 11973

E. Beier, H. Brody, R. Patton, K. Raychaudhuri, H. Takeda, R. Thern, and R. Van Berg
Department of Physics, University of Pennsylvania, Philadelphia, Pennsylvania 19104
(Received 2 December 1977)

Measurements of inclusive scattering in the target-fragmentation region are extended to higher incident energy. The combined data set shows departures from an approach to the asymptotic scaling limit as $A + Bs^{-1/2}$ that are significant even at the highest energies. When these departures are taken into account, the data approach a limit that is consistent with equal cross sections induced by particles and antiparticles and with Pomeron factorization. The corrections to $A + Bs^{-1/2}$ are so large that detailed tests of Mueller-Regge relationships are not conclusive.

I. INTRODUCTION

A study of the s dependence of proton fragmentation by hadrons is extended to Fermilab energies in this paper. In a previous paper,[1] hereafter referred to as I, measurements of cross sections $\Delta\sigma\,(ab \to c)$ for the production of particle c in the inclusive reaction $a+b \to c+$ anything where $a=(\pi^{\pm},K^{\pm},p^{\pm})$, $b=p$, and $c=(\pi^{\pm},K^{+},p)$, were reported for incident momenta $p_a^{\rm lab}$ in the range 4–24 GeV/c. The measurements were made in a small, fixed region of the phase space of particle c corresponding approximately to transverse momentum $p_T=0.3$ GeV/c and laboratory rapidity $y_L=0.6$, 0.4 and 0.2 for produced π, K, and p, respectively. In this paper data points at incident momenta $p_a^{\rm lab}=30$, 75, 150, and 250 GeV/c are added to the data set of paper I.

The data are analyzed using the Mueller-Regge phenomenology[2] which represents each inclusive cross section as the sum of an "asymptotic" term with a dependence on $s=(p_a+p_b)^2$ that is constant to within powers of $\log s$, and "secondary" terms that behave approximately as $s^{-1/2}$. The asymptotic term is the contribution of Pomeron exchange and the secondary terms arise from the exchange of the ρ, ω, A_2, and f Regge poles. Contributions from other Regge poles and more complicated singularities have an s dependence that falls much faster than $s^{-1/2}$ and are not expected to contribute to cross sections at sufficiently high energy. Such contributions will be referred to as "lower-lying" terms.

The question of the energy regime for the validity of this phenomenology is outside the theory and must be taken from experiment. In the case of hadron-hadron total cross sections (the inclusive reaction $a+b \to$ anything) high-energy behavior is found to begin at incident energies of a few GeV.[3,4] In the case of single-particle production, $a+b \to c+$ anything, much early work[5] has drawn optimistic conclusions about the validity of Mueller-Regge theory at similarly low energies.

The data of I, on the other hand, suggest that the range 4–24 GeV/c is too low for an extrapolation to the region of asymptotic behavior to be valid. With the addition of the higher-energy data in the present paper, it becomes obvious that there are large lower-lying contributions to the cross sections in the range of incident momenta from 30–250 GeV/c. These appear as significant departures from the energy dependence

$$\Delta\sigma = A + B\, s^{-1/2}. \tag{1}$$

The magnitude of these contributions at any given energy is estimated, and an attempt is made to extract the asymptotic behavior. It is found with little ambiguity that the high-energy limit confirms the prediction of equal asymptotic cross sections for incident particle and antiparticle to within a measurement accuracy of about 15% and the prediction of Pomeron factorization to about 10%.

The prediction of equal asymptotic cross sections for incident particle and antiparticle and the prediction of Pomeron factorization are not specific to the Mueller-Regge phenomenology. The phenomenology does, however, make unique predictions, based on Regge trajectories and residues determined from fits to the hadron-hadron total cross sections and exclusive reactions, about the coefficients B in Eq. (1). We find that the fitted values of the B coefficients have large uncertainties because of correlation with the large contribution of lower-lying terms to the energy dependence. Although the detailed Mueller-Regge pre-

dictions are consistent with the data, this consistency is not a stringent test of the phenomenology. It is shown that even with considerably more accurate data this effective unverifiability of the Mueller-Regge phenomenology would continue to hold true in our kinematic region.

In Sect. II aspects of the instrumentation of the experiment unique to Fermilab are discussed. Since the same spectrometer was used for the low-energy measurements at Brookhaven National Laboratory and for the high-energy measurements at Fermilab, any systematic differences in the measurements would be due to differences in the incident beam. For details of the reconstruction and identification of secondary particles, and the extraction of cross sections, the reader is referred to paper I. The measured cross sections, integrated over the acceptance of the spectrometer, are presented in Sec. III. This section also presents the conclusions of a phenomenological analysis of the s dependence of the cross sections.

II. EXPERIMENTAL TECHNIQUE

The spectrometer was installed in the 3.5-mrad $M1$-West beam of the Meson Laboratory at Fermilab. The beam had two intermediate foci and a final focus in both the horizontal and vertical planes. A collimator at the first focus defined the beam momentum. The momentum dispersion at this focus was 0.4%/cm. This collimator was adjusted to obtain a flux of 3×10^6 particles/sec at the final focus without affecting the beam-spot size. The momentum-analyzed beam was next brought to a momentum-recombined focus and then made parallel for particle identification. The momentum-recombined beam was brought to a final focus at a liquid-hydrogen target identical to the one described in paper I, at a distance of 503 m from the production target. A coincidence B of three circular scintillation counters, $B1$, $B2$, and $B3$, each 0.32 cm thick, and located 30, 4, and 0.07 m, respectively, upstream from the liquid-hydrogen target, defined a charged particle entering the hydrogen target.

The 19-nsec radio-frequency structure of the beam at Fermilab required special attention to avoid intensity-dependent absolute normalization errors. The signals from each of the three scintillators of the B telescope were split and the signals were discriminated just below single and double minimum-ionizing thresholds, respectively. Radio-frequency buckets populated by more than one beam particle produced pulses equal to or greater than twice minimum ionizing in all three scintillation counters. The threefold coincidence of double minimum ionizing beam signals in anti-

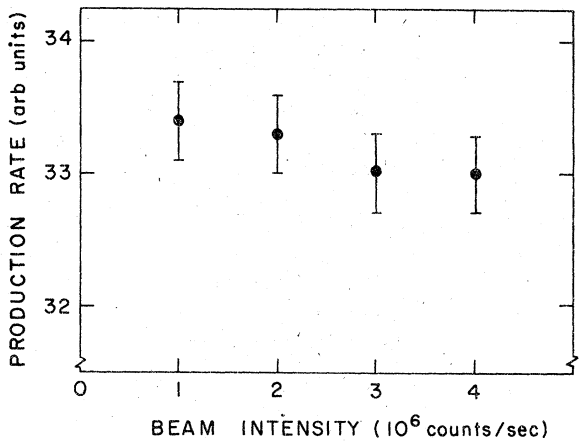

FIG. 1. Production rate of positively charged particles at 30° in the laboratory by a negative beam of momentum 75 GeV/c as a function of beam intensity. The empty-target background has been subtracted.

coincidence with the threefold coincidence of the signals from the lower threshold discriminators generated the beam coincidence B.

To test that the signal B included only singly populated radio-frequency buckets, the production rate of charged particles at $\theta_c^{\text{lab}} = 30°$ was measured as a function of beam intensity with all other conditions held fixed. The data in Fig. 1 show that the production rate was independent of intensity to 1% sensitivity up to 4×10^6 counts/second. For the Fermilab data reported in this paper the intensity was typically 3×10^6 counts/sec. At 3×10^6 counts/sec approximately 15% of the populated radio-frequency buckets were rejected. Furthermore, the average populations of the four radio-frequency buckets immediately preceding and following an event were monitored by time-to-digital converters. No correlation in the average populations was observed.

Simultaneous identification of the three types of beam particle (π, K, p) was provided by two high-resolution gas differential Čerenkov counters and a gas threshold Čerenkov counter in coincidence with the signal B from the beam telescope. At 30 and 75 GeV/c the two differential counters were set to define π and K, while the threshold counter was set to count both π and K. Protons and antiprotons were defined to be coincidences of the B telescope during which no Čerenkov counter responded. At 150 GeV/c the two differential counters were set to count K and p, respectively, and Čerenkov light at an angle greater than 5 mrad in the threshold counter identified pions. At 250 GeV/c, the K flux was too small to be useful in this experiment, so the differential counters were set to identify π and p and the threshold counter

was evacuated. For all incident momenta, the efficiencies of the counters were stable and the total efficiency of particle identification ranged from 75 to 95%. Misidentification of beam particle types was negligible.

Electrons were removed from the beam by 0.4 radiation lengths of lead inserted at the first focus of the beam. At 30 GeV/c the lead could not be used because its multiple scattering resulted in a large decrease in beam intensity, but at this momentum the electrons were easily resolved from pions by the differential Čerenkov counter that counted the pions.

The muon contamination of the pion signal was measured for each momentum and polarity by a crude ionization calorimeter. The calorimeter was constructed from three 0.61-m-thick blocks of steel followed by three 0.91-m-thick concrete shielding blocks. The pulse height in a 2.54-cm-thick plastic scintillator located after the second 0.61 m of steel was examined for all incident particles identified as pions by the Čerenkov counters in order to obtain the spectrum of pulse heights produced by a hadron cascade. A clear peak [Fig. 2(a)] in the spectrum corresponding to

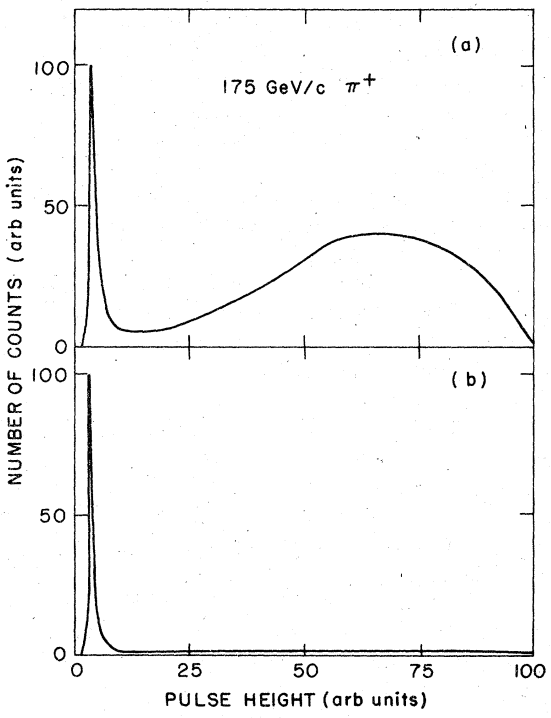

FIG. 2. Representation of pulse-height spectra for 175-GeV/c π^+ in the calorimeter: (a) spectrum for all beam particles identified as pions by the Čerenkov counters, (b) spectrum for all beam particles identified as pions which register a penetrating particle in a large counter behind the calorimeter.

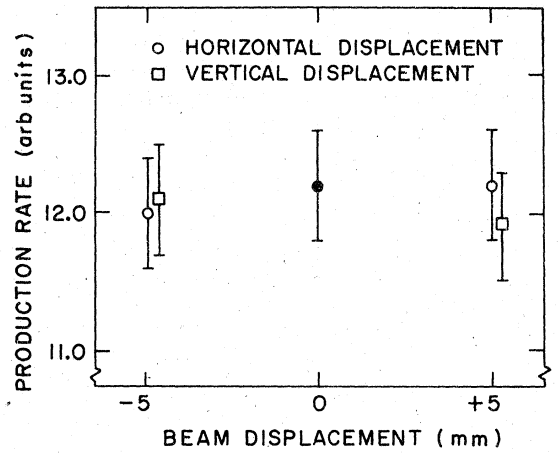

FIG. 3. Production rate of positively charged particles at 40° in the laboratory by a negative beam of momentum 150 GeV/c showing the effect of missteering the beam on the liquid-hydrogen target. The empty-target background has been subtracted.

muons, pions which had not interacted, and low-multiplicity events was observed below a continuum of large pulse heights corresponding to hadron cascade products. The pulse-height spectrum in the same counter was then measured for all particles which were identified as pions, and which penetrated (or had cascade products which penetrated) the entire calorimeter. This spectrum is displayed in Fig. 2(b). It indicates a minimum ionizing component due to muons identified as pions, and a component which was determined, by varying the size of the counter behind the calorimeter, to be hadron cascades which punch through the calorimeter. The procedure was repeated for incident protons, in which case there was no minimum-ionizing component. The measured μ/π ratio, corrected for pion decay between the liquid-hydrogen target and the calorimeter, was between 1.0 and 2.4%, and was used to correct the incident pion flux at each incident momentum.

The beam size at the liquid-hydrogen target varied with momentum from approximately 0.7-cm diameter to 1.2-cm diameter. The production rate of charged particles was measured at $\theta_c^{\rm lab} = 40°$ with the beam missteered by ± 0.5 cm in either direction. The data in Fig. 3 show that the measured production rates were independent of missteering to 3% sensitivity.

III. RESULTS AND ANALYSIS

A. Cross sections and errors

The cross sections measured in this experiment are differential cross sections integrated over the acceptance of the spectrometer, A, and integrated

over all azimuthal angles:

$$\Delta\sigma = \int_0^{2\pi} d\varphi \int_A d\theta\, dp \frac{d^3\sigma}{d\theta\, dp\, d\varphi}, \quad (2)$$

where p, θ, φ are the laboratory momentum and angles of the produced particle c. The limits of the acceptance, A, of the spectrometer used to detect the secondary particle c were the same as in the lower-energy work reported in paper I:

$$59.4^\circ \leq \theta_c^{\rm lab} + 3.4^\circ\,[(\text{GeV}/c)/(p_c^{\rm lab} - \Delta p_c)] \leq 64.4^\circ \quad (3a)$$

$$0.3\ \text{GeV}/c \leq p_c^{\rm lab} - \Delta p_c \leq 0.6\ \text{GeV}/c \quad (3b)$$

where $\Delta p_c \simeq (0.0015\ \text{GeV}/c)/\beta_c^3$ is the momentum lost by particle c before the momentum measurements, and β_c is its velocity.

The resolution of the spectrometer was inadequate for checking the absolute normalization of the measured cross sections by measuring elastic scattering cross sections at Fermilab energies. Consistency between the Fermilab and Brookhaven data sets was checked by examining the cross sections which have a weak dependence on s. In particular, the high-statistics, slowly varying cross sections for $pp \to \pi^\pm$, $\pi^+p \to \pi^-$, and $\pi^-p \to \pi^+$ exhibit no evidence for a shift of normalization between the two data sets to a systematic uncertainty corresponding to one standard deviation (2–4%).

The measured inelastic cross sections defined in Eq. (2) are tabulated in Table I. Cross sections for the production of K^- and $\bar{p}$ by $\pi^\pm$, $K^\pm$, and $p^\pm$ and cross sections for the production of K^+ by $K^\pm$ and $\bar{p}$ are below the sensitivity of this experiment. The error for each cross section in the table was obtained by adding in quadrature the statistical error and a point-to-point systematic error of 2%. The absolute normalization error is estimated to be 3% for $\pi^\pm$ and p production, and 15% for K^+ production; this overall normalization uncertainty

TABLE I. Cross sections $\Delta\sigma\,(ap \to c)$, integrated over the kinematic region of Eq. (3). The error given is the statistical error added in quadrature with a 2% point-to-point systematic error. An overall normalization error of 3% ($c = \pi^\pm, p$) or 15% ($c = K^+$) is not included.

a	$p_a^{\rm lab}$ (GeV/c)	$s^{-1/2}$ (GeV/c^{-1})	$\Delta\sigma\,(ap \to \pi^-)$ (μb)	$\Delta\sigma\,(ap \to \pi^+)$ (μb)	$\Delta\sigma\,(ap \to K^+)$ (μb)	$\Delta\sigma\,(ap \to p)$ (μb)
π^-	4	0.345	367 ± 17	284 ± 13	6.1 ± 1.5	145 ± 8
	6	0.287	311 ± 9	288 ± 9	5.2 ± 1.0	216 ± 7
	8	0.251	295 ± 9	304 ± 9	6.1 ± 1.3	181 ± 6
	10	0.225	268 ± 7	284 ± 8	3.6 ± 1.0	191 ± 6
	12	0.207	253 ± 7	281 ± 7	3.6 ± 0.8	185 ± 5
	15	0.186	239 ± 6	276 ± 7	7.4 ± 1.1	180 ± 5
	20	0.161	220 ± 6	275 ± 7	4.7 ± 1.0	154 ± 4
	24	0.148		257 ± 10	3.9 ± 1.6	154 ± 7
	30	0.132	213 ± 6	275 ± 7	5.1 ± 1.0	150 ± 4
	75	0.084	193 ± 5	277 ± 7	7.4 ± 0.9	149 ± 4
	150	0.060	192 ± 5	281 ± 7	5.0 ± 0.9	143 ± 4
π^+	4	0.345	133 ± 6	499 ± 18	5.9 ± 1.9	215 ± 8
	6	0.287	157 ± 6	464 ± 13	4.5 ± 1.4	303 ± 9
	8	0.251	157 ± 5	442 ± 12	3.7 ± 1.2	238 ± 8
	10	0.225	154 ± 6	389 ± 11	6.5 ± 1.7	249 ± 8
	12	0.207	149 ± 6	388 ± 12	5.3 ± 1.8	237 ± 8
	15	0.186	156 ± 10	341 ± 14	6.9 ± 3.2	221 ± 10
	20	0.161	173 ± 22	375 ± 22		182 ± 15
	30	0.132	155 ± 5	331 ± 9	5.7 ± 1.2	177 ± 5
	75	0.084	166 ± 5	303 ± 8	5.7 ± 1.3	162 ± 5
	150	0.060	160 ± 6	311 ± 9	5.2 ± 1.6	150 ± 5
	250	0.046	171 ± 11	306 ± 18	9.8 ± 4.4	156 ± 11
K^-	8	0.249	240 ± 67	208 ± 71		170 ± 40
	10	0.224	149 ± 36	283 ± 53		182 ± 32
	12	0.206	138 ± 26	237 ± 27		211 ± 25
	15	0.185	213 ± 36	184 ± 39		181 ± 27
	20	0.161	151 ± 37	241 ± 47		121 ± 30
	75	0.084	173 ± 13	241 ± 16		122 ± 10
	150	0.059	150 ± 13	211 ± 14		115 ± 11

TABLE I. (*continued*)

a	p_a^{lab} (GeV/c)	$s^{-1/2}$ (GeV/c^{-1})	$\Delta\sigma(ap\to\pi^-)$ (μb)	$\Delta\sigma(ap\to\pi^+)$ (μb)	$\Delta\sigma(ap\to K^+)$ (μb)	$\Delta\sigma(ap\to p)$ (μb)
K^+	8	0.249	99 ± 19	314 ± 51		132 ± 38
	10	0.224	100 ± 25	202 ± 34		153 ± 27
	12	0.206	98 ± 23	251 ± 33		199 ± 29
	15	0.185	79 ± 27	244 ± 46		68 ± 23
	20	0.161	210 ± 72	220 ± 53		195 ± 47
	75	0.084	132 ± 13	236 ± 18		145 ± 14
	150	0.059	159 ± 13	220 ± 17		137 ± 12
$\bar{p}$	8	0.243	937 ± 138	937 ± 118		351 ± 67
	10	0.220	654 ± 89	562 ± 98		350 ± 73
	12	0.203	644 ± 109	810 ± 94		382 ± 62
	15	0.183	532 ± 126	445 ± 168		457 ± 104
	20	0.159		792 ± 399		
	30	0.131	395 ± 24	586 ± 31		257 ± 19
	75	0.084	334 ± 19	564 ± 26		255 ± 16
	150	0.059	314 ± 30	481 ± 37		224 ± 21
p	4	0.325	101 ± 7	408 ± 13	5.5 ± 2.1	340 ± 12
	6	0.276	163 ± 8	408 ± 14	2.9 ± 1.7	374 ± 12
	8	0.243	184 ± 6	422 ± 13	5.5 ± 2.5	373 ± 12
	10	0.220	206 ± 7	422 ± 12	7.9 ± 1.8	317 ± 9
	12	0.203	210 ± 6	440 ± 11	5.1 ± 1.2	313 ± 8
	15	0.183	234 ± 7	450 ± 11	5.6 ± 1.2	293 ± 8
	20	0.159	245 ± 6	460 ± 10	5.2 ± 0.7	280 ± 6
	30	0.131	263 ± 10	457 ± 15	6.8 ± 2.3	265 ± 11
	75	0.084	252 ± 6	451 ± 10	11.4 ± 1.3	237 ± 6
	150	0.059	255 ± 7	453 ± 11	7.3 ± 1.2	233 ± 6
	250	0.046	269 ± 6	444 ± 10	10.6 ± 1.4	223 ± 6

is not included in Table I.

The same cross sections are plotted in Figs. 4(a)–4(d) as a function of $s^{-1/2}$ as suggested by the Mueller-Regge phenomenology. The smooth curves are Mueller-Regge fits to the data; the fits are discussed in Sec. III E.

B. The energy dependence of the cross sections

It is evident that the data do not, in general, lie on straight lines in Fig. 4 and thus that there are large departures from the energy dependence $A+Bs^{-1/2}$. To exhibit these departures more clearly, Figs. 5(a)–5(c) show the same cross sections replotted for the cases where both the beam particle a and detected particle c are chosen among the copiously produced particles $\pi^\pm$ and p^+; the data for these reactions have high statistical accuracy.

There is little theoretical guidance to the kinematic range of s, y_L, and p_T over which the Mueller-Regge behavior is expected to apply. If the departure from $A+Bs^{-1/2}$ is due to lower-lying Regge-pole contributions, we expect terms in s^{-1}, while contributions from Regge cuts would involve complicated logarithmic functions. Alternatively, the Mueller-Regge behavior, even with the corrections above, may not hold in all or part of the kinematic region investigated in this work. Since it is not possible with the present data to distinguish these possibilities, we have represented the corrections to the expression $A+Bs^{-1/2}$ by the term Cs^{-1} for the production of $\pi^\pm$ by $\pi^\pm$ and p. Fits to

$$\Delta\sigma = A + Bs^{-1/2} + Cs^{-1} \tag{4}$$

over the momentum interval $4 \leq P_a^{lab} \leq 250$ GeV/c are tabulated in Table II and represented by the solid lines in Figs. 5(a) and 5(b). The data on pion production by $\pi^\pm$ and p are well represented by this expression.

The Mueller-Regge energy dependence should then be determined by the component $A+Bs^{-1/2}$ of the fit. This component is shown in Figs. 5(a) and 5(b) as dotted lines. However, it can be seen from Table II that the B coefficients are not well determined because of the correlations between the B and C terms. Furthermore, the statistical errors underestimate the true uncertainty in the coefficients because the uncertainty in the functional form of the correction to $A+Bs^{-1/2}$ leads to an un-

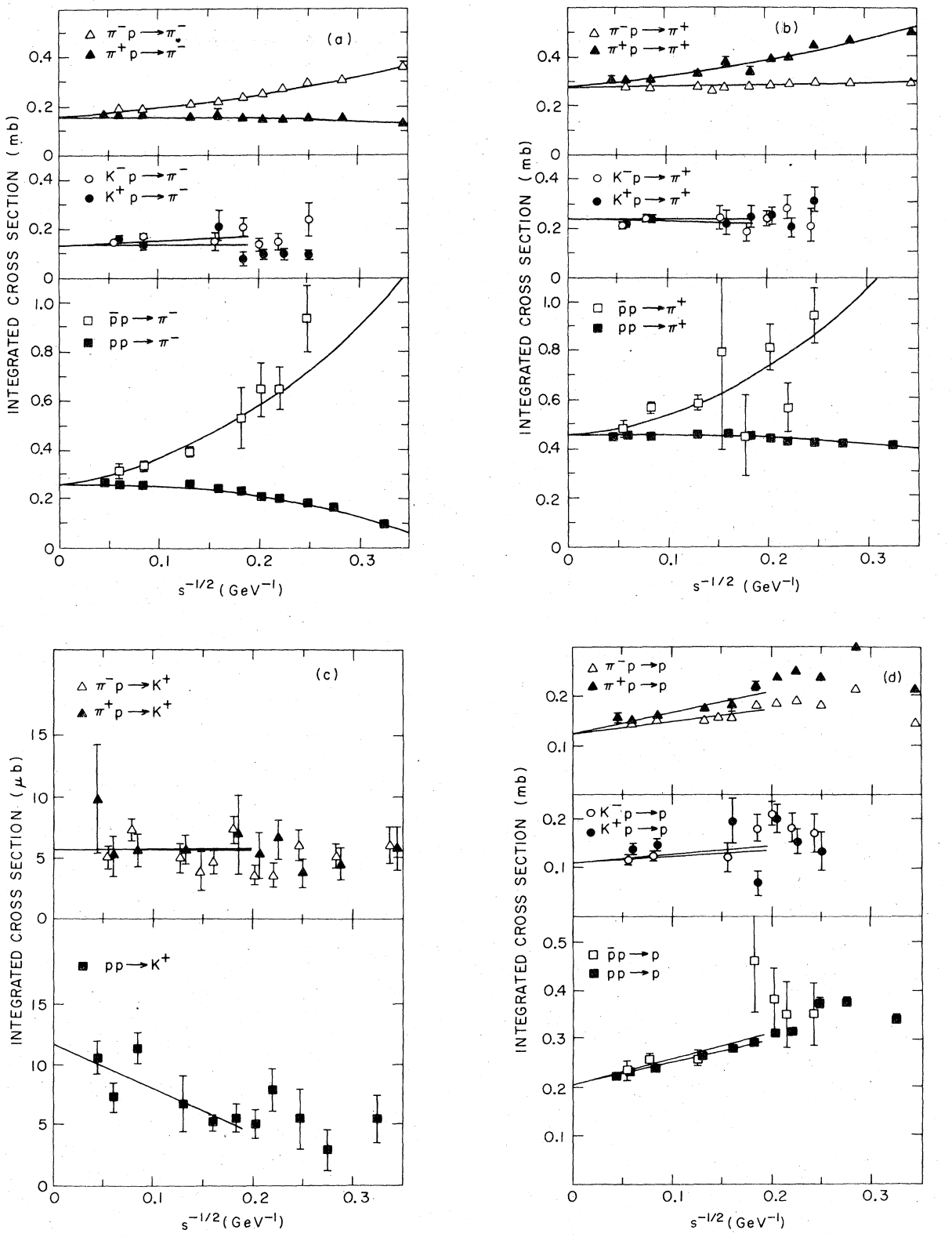

FIG. 4. Cross sections, integrated over the kinematic region in Eq. (3), for the production of (a) π^-, (b) π^+, (c) K^+, and (d) p. The solid lines in (a), (b), and (d) are Mueller-Regge fits from Table VIII and those in (c) are from Table V. Where two symbols overlap, the negative-beam signal has been displaced to the left.

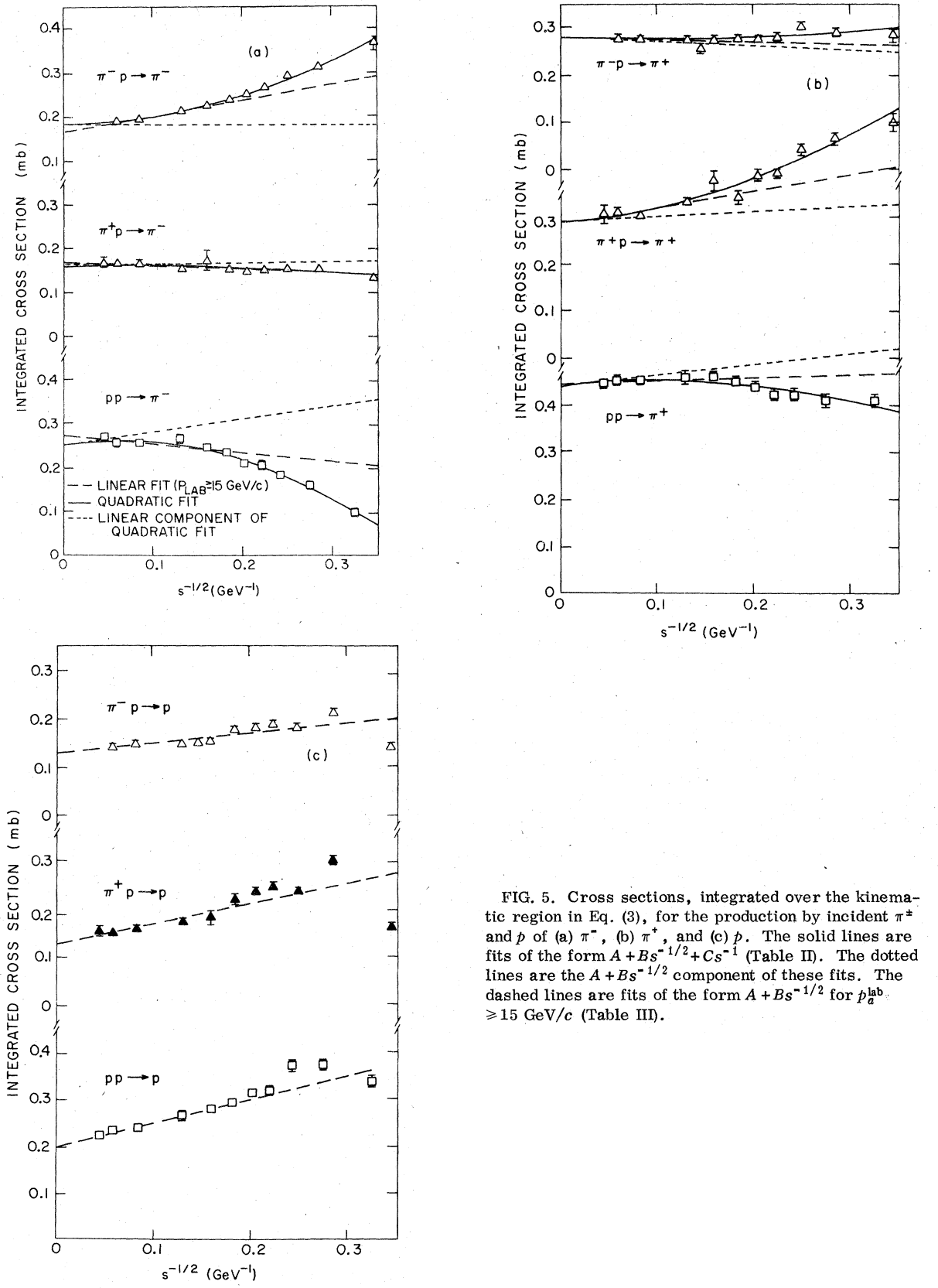

FIG. 5. Cross sections, integrated over the kinematic region in Eq. (3), for the production by incident $\pi^\pm$ and p of (a) π^-, (b) π^+, and (c) p. The solid lines are fits of the form $A + Bs^{-1/2} + Cs^{-1}$ (Table II). The dotted lines are the $A + Bs^{-1/2}$ component of these fits. The dashed lines are fits of the form $A + Bs^{-1/2}$ for $p_a^{\text{lab}} \geq 15$ GeV/c (Table III).

TABLE II. Fits of Eq. (4) to the data for $a = \pi^{\pm}, p$ and $c = \pi^{\pm}$. The fits were carried out over the momentum range $4 \leqslant p_c^{\text{lab}} \leqslant 250$ GeV/c.

Reaction	A (μb)	B (μb GeV)	C (μb GeV^2)	χ^2	DF
$\pi^- p \to \pi^-$	184 ± 9	−9 ± 125	1630 ± 370	3.3	7
$\pi^+ p \to \pi^-$	162 ± 8	33 ± 95	−280 ± 250	9.0	8
$p p \to \pi^-$	251 ± 8	312 ± 100	−2370 ± 280	8.8	8
$\pi^- p \to \pi^+$	281 ± 11	−89 ± 135	420 ± 370	10.9	8
$\pi^+ p \to \pi^+$	291 ± 15	107 ± 191	1630 ± 530	12.9	8
$p p \to \pi^+$	442 ± 13	221 ± 173	−1110 ± 500	5.1	8

known systematic error in the B and C terms. To represent the uncertainty in the B coefficients in a different way the data have been fitted by Eq. (1) for $p_a^{\text{lab}} \geq 15$ GeV/c (Table III). With this low-energy cutoff the fit quality is just as high as that in Table II. The resulting fits are shown in Fig. 5 as dashed lines.

Comparing the dashed and dotted lines in Figs. 5(a) and 5(b), one can see that the intercepts agree well but the slopes are in general quite different. Thus, *the high-energy limits of the cross sections for pion production are well determined by the data, but the rate of approach to this asymptotic limit is only poorly determined.*

When particle c is a pion or kaon, the missing mass $m_x = [(p_a + p_b - p_c)^2]^{1/2}$ is always greater than 2.5 GeV/c^2 in the kinematic region of this experiment. However, when c is a proton and the incoming momentum p_a^{lab} is below 15 GeV/c, m_x can be in the resonance region where the Mueller-Regge theory would not be expected to apply. Indeed, in Fig. 5(c) there is significant resonant structure below 15 GeV/c from reactions such as $\pi p \to pA_2$ and $pp \to pN^*$. Therefore, only the $A + Bs^{-1/2}$ fits for $p_a^{\text{lab}} \geq 15$ GeV/c [Table III and dashed lines in Fig. 5(c)] are presented for produced protons.

C. Asymptotic properties of the cross sections

It is evident from Fig. 4 that the particle- and antiparticle-induced cross sections, $\Delta\sigma(ap \to c)$ and $\Delta\sigma(\bar{a}p \to c)$, approach each other in the asymptotic limit $s \to \infty$ or $s^{-1/2} \to 0$. Although analogous behavior for the total cross sections is required by the Pomeranchuk theorem, there is no such *a priori* constraint for the single-particle inclusive cross sections. This behavior will occur if the asymptotic cross section, which is related by the Mueller theorem to a three-body scattering amplitude, is even under the operation of replacing the projectile, a, with its antiparticle conjugate, $\bar{a}$. On the other hand, if the asymptotic contribution has a part which is odd under the operation $a \to \bar{a}$, the particle and antiparticle induced reactions will not be asymptotically equal. In the Mueller-Regge phenomenology the asymptotic cross section is determined by Pomeron exchange and is even under the operation $a \to \bar{a}$.

Quantitative tests of the equality of the asymp-

TABLE III. Fits of Eq. (1) to the data. The fits were carried out over the momentum range $15 \leqslant p_a^{\text{lab}} \leqslant 250$ GeV/c.

Reaction	A (μb)	B (μb GeV)	χ^2	DF
$\pi^- p \to \pi^-$	167 ± 7	354 ± 53	2.4	3
$\pi^+ p \to \pi^-$	169 ± 7	−77 ± 69	2.4	4
$K^- p \to \pi^-$	137 ± 23	323 ± 252	2.0	2
$K^+ p \to \pi^-$	185 ± 22	−541 ± 234	3.0	2
$\bar{p} p \to \pi^-$	229 ± 47	1286 ± 474	0.4	2
$pp \to \pi^-$	272 ± 6	−185 ± 53	4.6	4
$\pi^- p \to \pi^+$	281 ± 9	−51 ± 64	3.5	4
$\pi^+ p \to \pi^+$	284 ± 12	347 ± 106	4.9	4
$K^- p \to \pi^+$	226 ± 25	−42 ± 283	3.2	3
$K^+ p \to \pi^+$	216 ± 30	142 ± 332	0.4	2
$\bar{p} p \to \pi^+$	460 ± 60	967 ± 602	3.2	3
$pp \to \pi^+$	446 ± 10	56 ± 86	0.9	4
$\pi^- p \to K^+$	5.7 ± 1.2	0.2 ± 9.4	8.3	4
$\pi^+ p \to K^+$	5.5 ± 2.2	2.0 ± 19.9	1.1	3
$pp \to K^+$	11.8 ± 1.2	−37.8 ± 9.3	9.6	4
$\pi^- p \to p$	130 ± 5	201 ± 40	13.7	4
$\pi^+ p \to p$	126 ± 7	421 ± 69	5.1	4
$K^- p \to p$	92 ± 18	371 ± 199	1.6	2
$K^+ p \to p$	170 ± 19	−427 ± 197	5.9	2
$\bar{p} p \to p$	201 ± 35	520 ± 352	3.9	2
$pp \to p$	200 ± 6	503 ± 54	1.1	4

TABLE IV. The asymptotic ratios of particle and antiparticle induced cross sections. The cross-section limits A_+ and A_- are taken from Table II for the production of $\pi^{\pm}$ by $\pi^{\pm}$ and p, and from Table III for the other reactions.

Cross-section ratio	$c = \pi^-$	$c = \pi^+$	$c = K^+$	$c = p$
$(\pi^+ p \to c)/(\pi^- p \to c)$	0.88 ± 0.06	1.04 ± 0.07	0.96 ± 0.04	0.97 ± 0.07
$(K^+ p \to c)/(K^- p \to c)$	1.35 ± 0.28	0.96 ± 0.17	...	1.86 ± 0.42
$(pp \to c)/(\bar{p} p \to c)$	1.10 ± 0.23	0.96 ± 0.13	...	0.99 ± 0.17

totic particle and antiparticle induced cross sections are given in Table IV. In this table the ratios A_+/A_- of the fitted asymptotic limits of the cross sections are given, where the limits A_+ and A_- were taken from Table II for the production of $\pi^\pm$ by $\pi^\pm$ and p, and from Table III for the other reactions. It can be seen that in every case the ratio is consistent with unity. For the cases where

TABLE V. Fits of Eq. (1) or Eq. (4) to the data. The intercept A is constrained to be the same for incident particle and antiparticle. For reactions in which the incident particle a is $\pi^\pm$ or $p^\pm$ and the produced particle c is $\pi^\pm$, Eq. (4) has been fitted to the data for $4 \leqslant p_a^{\text{lab}} \leqslant 250$ GeV/c; for the other reactions Eq. (1) has been fitted to the data for $15 \leqslant p_a^{\text{lab}} \leqslant 250$ Gev/c.

Reaction	A (μb)	B (μb GeV)	C (μb GeV^2)	χ^2	DF
$\pi^- p \to \pi^-$		158 ± 87	1180 ± 280		
	171 ± 6			15.7	16
$\pi^+ p \to \pi^-$		-73 ± 76	-30 ± 210		
$K^- p \to \pi^-$		64 ± 187	...		
	162 ± 16			7.3	5
$K^+ p \to \pi^-$		-314 ± 182	...		
$\bar{p} p \to \pi^-$		224 ± 363	7850 ± 2440		
	252 ± 8			11.8	13
$pp \to \pi^-$		301 ± 99	-2340 ± 280		
Total $ap \to \pi^-$				34.8	34
$\pi^- p \to \pi^+$		-132 ± 110	520 ± 310		
	284 ± 9			24.1	17
$\pi^+ p \to \pi^+$		184 ± 129	1430 ± 390		
$K^- p \to \pi^+$		0 ± 227	...		
	222 ± 19			3.6	5
$K^+ p \to \pi^+$		84 ± 240	...		
$\bar{p} p \to \pi^+$		1029 ± 459	1360 ± 2710		
	442 ± 13			15.1	14
$pp \to \pi^+$		217 ± 172	-1100 ± 490		
Total $ap \to \pi^+$				42.8	36
$\pi^- p \to K^+$		0.6 ± 8.4	...		
	5.7 ± 1.1			9.4	9
$\pi^+ p \to K^+$		0.3 ± 11.2	...		
$pp \to K^+$	11.8 ± 1.2	-37.8 ± 9.3	...	9.6	4
Total $ap \to K^+$				19.0	13
$\pi^- p \to p$		209 ± 34	...		
	129 ± 4			19.0	9
$\pi^+ p \to p$		400 ± 45	...		
$K^- p \to p$		-5 ± 154	...		
	129 ± 13			16.4	5
$K^+ p \to p$		-44 ± 149	...		
$\bar{p} p \to p$		532 ± 120	...		
	200 ± 6			5.0	7
$pp \to p$		503 ± 53	...		
Total $ap \to p$				40.4	21

TABLE VI. Tests of Pomeron factorization, Eq. (5).

Cross-section ratio	$c=\pi^-$	$c=\pi^+$	$c=K^+$	$c=p$	Predicted ratio (Ref. 4)
$(\pi p\to c)/(pp\to c)$	0.68 ± 0.03	0.64 ± 0.03	0.48 ± 0.11	0.64 ± 0.03	0.61 ± 0.02
$(Kp\to c)/(pp\to c)$	0.64 ± 0.07	0.50 ± 0.05		0.65 ± 0.07	0.53 ± 0.02

both a and c are $\pi^\pm$ or p, the two standard deviation accuracy of the test is about 15%. In the further analyses of the data, it will be assumed that particle and antiparticle cross sections are equal at $s^{-1/2}=0$.

Table V gives the coefficients of fits to the data in which the A parameter is assumed to be the same for incident particle and antiparticle. In these fits Eq. (4) has been used to fit the data over the range $4\leq p_a^{\rm lab}\leq 250$ GeV/c for the reactions where $a=\pi^\pm$ or $p^\pm$ and $c=\pi^\pm$; otherwise, Eq. (1) has been used to fit the data for $P_a^{\rm lab}\geq 15$ GeV/c only.

According to Pomeron factorization

$$\lim_{s\to\infty}\frac{\Delta\sigma(a'p\to c)}{\Delta\sigma(ap\to c)}=\lim_{s\to\infty}\frac{\sigma_T(a'p)}{\sigma_T(ap)}, \tag{5}$$

where $\sigma_T(ap)$ represents the ap total cross section. A theoretical ambiguity arises because of the experimentally observed[3] high-energy rise in the hadron-hadron total cross sections. The observed amount of rise in σ_T over the present energy range is not large, and an equivalent rise in the inclusive cross sections $\Delta\sigma$ would not be seen in this experiment, but an ambiguity arises in the meaning of the high-energy limit. In the analysis of the total cross sections,[4] the rising part of the total cross section has been parametrized by

$$D_{ap}=K_{ap}\ln[(p_a^{lab}+m_a)/b_a], \tag{6}$$

where K_{ap}, m_a, and b_a are constants given in Ref. 4. We have evaluated the right-hand side of Eq. (5) using $\sigma_T(ap)=D_{ap}$ and $P_a^{\rm lab}=250$ GeV/c. The left-hand side of Eq. (5) was evaluated using the fits of Table V.

The resulting predictions are compared with experiment in Table VI. The quoted error in the predictions is statistical only, and does not include an allowance for theoretical ambiguities. The two-standard-deviation experimental errors are about 10% for $a, c=\pi^\pm$ or p. At this level of accuracy, the data agree with Pomeron factorization.

D. Differences between cross sections induced by particles and their antiparticles

At asymptotic energies, the difference between particle- and antiparticle-induced cross sections goes to zero:

$$\Delta_{ab}(c)\equiv\Delta\sigma(ab\to c)-\Delta\sigma(\bar a b\to c)\underset{s\to\infty}{\longrightarrow}0. \tag{7}$$

The specific way in which $\Delta_{ab}(c)$ approaches zero contains information about inclusive interactions in general and the Mueller-Regge phenomenology in particular.

First, consider the case where particle a is a proton or antiproton. The $\bar pp$ interaction has two components: annihilation (no baryons in the final state) and scattering. The pp interaction, however, has no annihilation component. Therefore, the annihilation process will contribute in general to $\Delta_{\bar pp}(c)$, and indeed it is evident from Figs. 4(a) and 4(b) that $\Delta_{\bar pp}(\pi^\pm)$ is large. However, the contribution from annihilation processes when particle c is a proton is suppressed or forbidden by energy-momentum conservation for the kinematic conditions (target fragmentation) of this experiment. It can be seen in Fig. 4(d) that $\Delta_{\bar pp}(p)$ is, in fact, small.

Next, consider the case where $a=\pi^\pm$. The data of this experiment determine the cross-section difference $\Delta_{\pi p}(c)$ reasonably well. These difference cross sections are plotted in Fig. 6 for $c=\pi^-$, π^+, and p. In the Mueller-Regge model, these differences are determined by exchange of the ρ trajectory and have the form

$$\Delta_{\pi p}(c)=Ds^{\alpha_\rho(0)-1}. \tag{8}$$

In the analysis of total-cross-section data,[4] the corresponding difference $\sigma_T(\pi^-p)-\sigma_T(\pi^+p)$ is well described by this form with $\alpha_\rho(0)$ near the value 0.5 which is needed for consistency with Regge analyses of exclusive reactions such as $\pi^-p\to\pi^0n$.

The data for $\pi^\pm$ and p production were fitted to Eq. (8) for $4\leq p_a^{\rm lab}\leq 150$ GeV/c. [The statistical errors on $\Delta_{\pi p}(p)$ are comparable to the resonance fluctuations in the difference cross section so the fit can reasonably be extended to 4 GeV/c to get an "average" s dependence.] The results of the fit are displayed in Table VII. The data are well described by Eq. (8), but with values of $\alpha_\rho(0)$ which differ significantly from 0.5.

These data are described equally well by the alternate expression

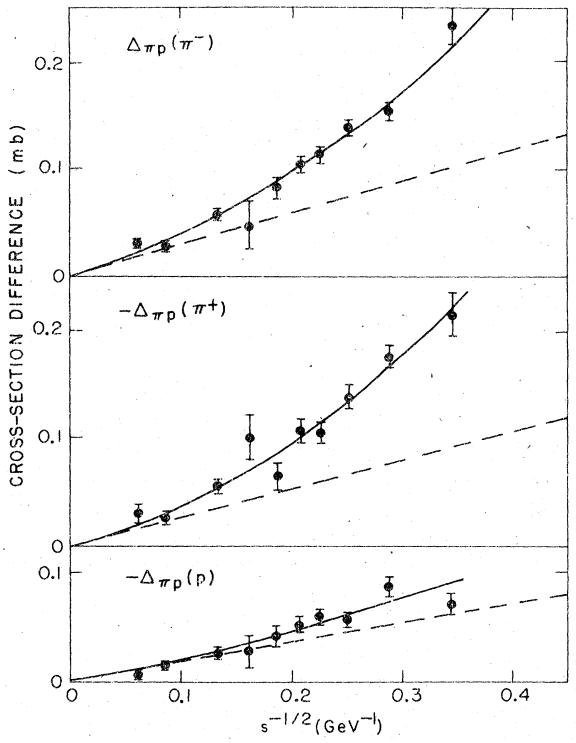

FIG. 6. Plots of the cross-section differences $\Delta_{\pi p}(c) \equiv \Delta\sigma(\pi^- p \to c) - \Delta\sigma(\pi^+ p \to c)$ for $c = \pi^-$, π^+, and p. The solid curves are fits (see Table VII) to Eq. (9) and the dashed lines are the $Bs^{-1/2}$ component of these fits. Fits of Eq. (8) would be indistinguishable from the solid curves shown.

$$\Delta_{\pi p}(c) = Bs^{-1/2} + Cs^{-1} \tag{9}$$

representing the sum of ρ-exchange and correction terms with the same quantum numbers as the ρ. The coefficients of this alternate fit are also given in Table VII. The fit is shown as the solid curves in Fig. 6 and its $Bs^{-1/2}$ component is shown as the dashed lines. The fit to Eq. (8) is not visibly different from the solid curves in Fig. 6; it is essentially impossible to discriminate experimentally between these functional forms.

If we adopt the point of view that the cross section differences are composed of a leading Regge term with $\alpha_\rho(0) \simeq 0.5$ plus lower-lying corrections, then Fig. 6 indicates that for pion production at $p_a^{\rm lab} = 15$ GeV/c these corrections contribute about 40% of the total difference cross section and at $p_a^{\rm lab} = 150$ GeV/c they still contribute about 20%. We also note that from Fig. 6, the relative correction term is about 3 times smaller for proton production ($y_L \simeq 0.2$) than for pion production ($y_L \simeq 0.6$).

E. Further tests of detailed Mueller-Regge predictions

The Mueller-Regge phenomenology suggests that the data of this experiment be described by

$$\Delta\sigma(ap \to c) = \beta_{pc}^P \gamma_a^P + \left(\sum_{R=f,\rho,\omega,A_2} \beta_{pc}^R \gamma_a^R \right) s^{-1/2} + C_{ap} s^{-1}. \tag{10}$$

This formula follows from Eq. (3) of I for $\alpha_\rho(0) = 1.0$ and $\alpha_R(0) = 0.5$, with the addition of Cs^{-1} terms to account for lower-lying corrections. The quantities γ_a^R in Eq. (10) are determined by total-cross-section measurements. From the total-cross-section analysis of Ref. 4, and assuming ρ universality, ω universality, f-ω exchange degeneracy, and ρ-A_2 exchange degeneracy, we find [in units of (mb)$^{1/2}$]

$$\gamma = \begin{bmatrix} 3.8 & 3.8 & 3.3 & 3.3 & 6.3 & 6.3 \\ 3.4 & 3.4 & 1.6 & 1.6 & 4.9 & 4.9 \\ 2.3 & -2.3 & 1.15 & -1.15 & 1.15 & -1.15 \\ 0.0 & 0.0 & 1.6 & -1.6 & 4.9 & -4.9 \\ 0.0 & 0.0 & 1.15 & 1.15 & 1.15 & 1.15 \end{bmatrix}, \tag{11}$$

where the rows correspond to P, f, ρ, ω, and A_2 exchange and the columns correspond to π^-, π^+, K^-, K^+, p^-, and p^+ incident. The Pomeron couplings are obtained from Eq. (6) evaluated at 250 GeV/c.

Coefficients of fits of Eq. (10) to the π^-, π^+, and p production data are presented in Table VIII. In these fits the Cs^{-1} term was included and the data were fitted over the complete energy range 4

TABLE VII. Fits of Eq. (8) and Eq. (9) to the cross-section differences $\Delta_{\pi p}(c) = \Delta\sigma(\pi^- p \to c) - \Delta\sigma(\pi^+ p \to c)$, for $c = \pi^\pm$ and p. The fits were carried out over the momentum range $4 \leq p_a^{\rm lab} \leq 150$ GeV/c.

	Fit to Eq. (8)				Fit to Eq. (9)			
c	D (μb GeV$^{2-2\alpha}$)	$\alpha_\rho(0)$	χ^2	DF	B (μb GeV)	C (μb GeV^2)	χ^2	DF
π^-	940 ± 150	0.31 ± 0.05	7.5	8	280 ± 60	1010 ± 250	5.8	8
π^+	-990 ± 220	0.28 ± 0.06	6.5	8	-270 ± 90	-1060 ± 350	5.9	8
p	-190 ± 50	0.39 ± 0.08	6.7	8	-190 ± 50	-170 ± 200	6.7	8

TABLE VIII. Fits to the data of the Mueller-Regge model Eq. (10) for $c = \pi^-$ and p^+. The momentum range for each reaction over which the fit was performed is discussed in the text.

	$c = \pi^-$	$c = \pi^+$	$c = p^+$
β^P_{pc} ($mb^{1/2}$)	0.0420 ± 0.0010	0.0721 ± 0.0015	0.0328 ± 0.0007
β^f_{pc} ($mb^{1/2}$ GeV)	0.052 ± 0.015	0.048 ± 0.023	0.098 ± 0.008
β^ρ_{pc} ($mb^{1/2}$ GeV)	0.056 ± 0.012	−0.074 ± 0.018	−0.042 ± 0.007
β^ω_{pc} ($mb^{1/2}$ GeV)	0.015 ± 0.015	0.025 ± 0.021	0.018 ± 0.009
$\beta^{A_2}_{pc}$ ($mb^{1/2}$ GeV)	0.024 ± 0.056	−0.123 ± 0.070	0.003 ± 0.036
$C_{\pi^- p}$ (μb GeV^2)	770 ± 220	200 ± 250	...
$C_{\pi^+ p}$ (μb GeV^2)	−300 ± 160	1030 ± 330	...
$C_{p\bar{p}}$ (μb GeV^2)	5920 ± 1240	6200 ± 1400	...
C_{pp} (μb GeV^2)	−1940 ± 240	−650 ± 400	...
χ^2	47.2	49.3	46.2
DF	38	40	25

$\leq p_a^{lab} \leq 250$ GeV/c for the reactions with $a = \pi^\pm$ or $p^\pm$ and $c = \pi^\pm$. For the remaining reactions the Cs^{-1} term was omitted and the data were fitted for 15 $\leq p_a^{lab} \leq 250$ GeV/c. The fitted energy dependence is shown in Figs. 4(a), 4(b), and 4(d) as the solid curves; for Fig. 4(c) (K^+ production) the fit of Table V is used. The resulting fit quality is not significantly worse than that of the fits to Eqs. (1) or (4) given in Table V, and thus the data are consistent with the Mueller-Regge theory.

Whether this consistency represents a significant confirmation of the theory depends, however, on a detailed error analysis. For a given produced particle c, we have measured and parametrized the cross sections for reactions with six different incident particles a. We have already seen that the data are consistent with Pomeron factorization, and therefore that the energy-independent part of the cross sections can be expressed successfully in terms of a single parameter β^P_{pc} of Eq. (10) instead of three independent parameters $A_{ap\to c}$ of Eqs. (1) or (4). In addition, the part of the cross section that varies as $s^{-1/2}$ is expressed in Eq. (10) in terms of four parameters β^R_{pc} instead of six parameters $B_{a^\pm p\to c}$ of Eqs. (1) or (4). The two resulting linear relationships for each produced particle c are the unique features of the Mueller-Regge phenomenology that are tested by the present data.

Detailed error analysis shows, however, that the resulting tests are not stringent, and that, with data of the present accuracy, the fit quality is not very sensitive to the actual energy dependence. That this is so is reflected in the large uncertainty in the A_2 residues in Table VIII, and in the fact that both the ω and the A_2 residues are statistically consistent with zero.

The reasons for the lack of stringency of the tests of the theory are as follows: (1) The reactions with minority beam particles $a = K^\pm$ or p^- have been measured with poor statistical accuracy and (2) the presence of large corrections to Eq. (1) introduces large fitting uncertainties in the determination of the coefficients of the $s^{-1/2}$ terms in the energy dependence. Error analysis of a hypothetical experiment in which minority-beam-particle reactions are measured as accurately as the others shows that the sensitivity to the theoretical linear relationships is improved by about a factor of 2, and the test of theory is still not decisive. Indeed, it appears that, in the present kinematic region, the Mueller-Regge phenomenology is effectively unverifiable.

F. Comparison with other experiments

Extensive results on the s dependence of proton fragmentation by hadrons have been obtained in bubble-chamber experiments.[6] To get adequate statistical accuracy, the data are integrated over a large region of phase space, for example $-0.4 < p_L < 0.2$ GeV/c and $0 < p_\perp < \infty$, so a direct compari-

son with the present work cannot be made. There is qualitative agreement, however, on the presence of nonleading corrections to the proton- and antiproton-induced reactions, and on the approximate validity of Pomeron factorization in the high-energy limit. Owing to the relatively large statistical and systematic errors, no quantitative analysis of the type presented here was given. Also, the nonleading terms in the pion-induced reactions were not seen.

G. Summary and conclusions

For single-particle inclusive scattering in a specific part of the target-fragmentation region, we have demonstrated that corrections to the simple Mueller-Regge s dependence, $A+Bs^{-1/2}$, are required. Nonetheless, the data support two conclusions about the asymptotic cross sections: (1) Particle- and antiparticle-induced cross sections approach the same asymptotic limit, and (2) the ratios of π, K, and p induced cross sections approach the same limits as the ratios of the π, K, and p total cross sections. The differences between particle- and antiparticle-induced cross sections approach their asymptotic limit in a manner which qualitatively supports the Mueller-Regge model; quantitative analysis, however, shows the existence of large correction terms in the phase region of this experiment. The data are shown to be consistent with the Mueller-Regge model, but do not put strong constraints on the model. Extended studies in other regions of (y_L, p_T) phase space are in progress.

ACKNOWLEDGMENTS

The cooperation and effort of the Meson Laboratory at Fermilab under P. Koehler, C. Brown, and T. Toohig are appreciated. This research was supported in part by the U.S. Department of Energy.

---

[1]E. W. Beier *et al.*, preceding paper, Phys. Rev. D 17, 2864 (1978).
[2]See Refs. 1–3 of the preceding paper.
[3]U. Amaldi *et al.*, Phys. Lett. 44B, 112 (1973); S. R. Amendolia *et al.*, *ibid.* 44B, 119 (1973); Nuovo Cimento 17A, 735 (1973); A. S. Carroll *et al.*, Phys. Rev. Lett. 33, 928 (1974); 33, 932 (1974).
[4]R. E. Hendrick *et al.*, Phys. Rev. D 11, 536 (1975).
[5]See, for example, M. S. Chen *et al.*, Phys. Rev. Lett. 26, 1585 (1971); H. Miettinen, Phys. Lett. 38B, 431 (1972); R. C. Brower, R. N. Cahn, and J. Ellis, Phys. Rev. D 7, 2080 (1973).
[6]See Ref. 9 of the preceding paper.